 DOI: 10.1002/masy.201000138

High-Resolution Tip-Enhanced Raman Mapping

G. G. Hoffmann,[*1] *L. Xue,*[1] *J. Loos,*[1,2] *G. de With*[1]

Summary: Tip-enhanced Raman mapping (TERM) can be used to obtain chemical analysis of a sample with a topographical resolution down to 15 nm. A short review of this technique is given. Among other samples (e.g. carbon nanotubes and graphene), we recently measured a high resolution tip-enhanced Raman map of a polymer for the first time. Using TERM, the phase separation behaviour of a polymer blend (PMMA/SAN) was monitored. In the early, incomplete state of phase separation an interface width of ~200 nm was measured. A spatial resolution in the tens of nm range could be achieved.

Keywords: atomic force microscopy (AFM); block copolymers; raman spectroscopy; Tip-enhanced raman mapping (TERM); Tip-enhanced raman spectroscopy (TERS); tip-etching

Introduction

Tip-enhanced Raman spectroscopy (TERS)[1–6] is the combination of two well known techniques: atomic force microscopy and Raman spectroscopy. Atomic force microscopy provides high spatial resolution and Raman spectroscopy enables chemical analysis of the sample.

From the well-filled basket of atomic force microscopy (AFM) technologies, mainly two methods are employed for tip-enhanced Raman spectroscopy: tapping mode and shear force mode. Using the tapping mode, a cantilever is excited to one of its resonance frequencies and the amplitude of this vibration is monitored. If the tip of the cantilever is then lowered, upon interaction in the vicinity of the sample its vibration is attenuated, and, by keeping the attenuation constant and providing feedback to the Z piezo drive, the distance to the sample is also kept constant. By scanning the sample and monitoring the height of the cantilever, a height profile of the sample is obtained. If the tip of the cantilever is now covered by gold or silver, the TER spectrum of the sample can also be recorded. If one wants to attach a larger probe to the scanning device, e.g. a pointed glass fiber or a metal wire, a tuning fork is much better suited. This is mostly operated in the shear force mode. In this mode the probe is also vibrating, but not vertically as in the tapping mode. Instead it is vibrating horizontally, thereby measuring the shear force interacting with the sample.

Raman spectroscopy[7,8] is well known for its applicability to the structure elucidation of small molecules as well as polymers, and it can even determine the chirality of molecules.[9,10] Even temperature measurements are possible from the different intensities of corresponding bands in the Stokes and *anti*-Stokes part of the spectrum.

The usefulness of Raman spectroscopy is greatly enhanced by the possibility to calculate vibrational spectra with high accuracy, and then to compare the results with the experiment. As an example, the calculated spectra of benzene are given as the spectra b) and c) in Figure 1. The theoretical spectra of the compound were calculated by density functional theory (DFT) on optimized geometries using Gaussian09[11] and the hybrid functional

[1] Laboratory of Materials and Interface Chemistry, Eindhoven University of Technology, 5600 MB Eindhoven, The Netherlands
E-mail: g.g.hoffmann@tue.nl
[2] present address: Department of Physics and Astronomy, University of Glasgow, Glasgow G12 8QQ, Scotland, United Kingdom

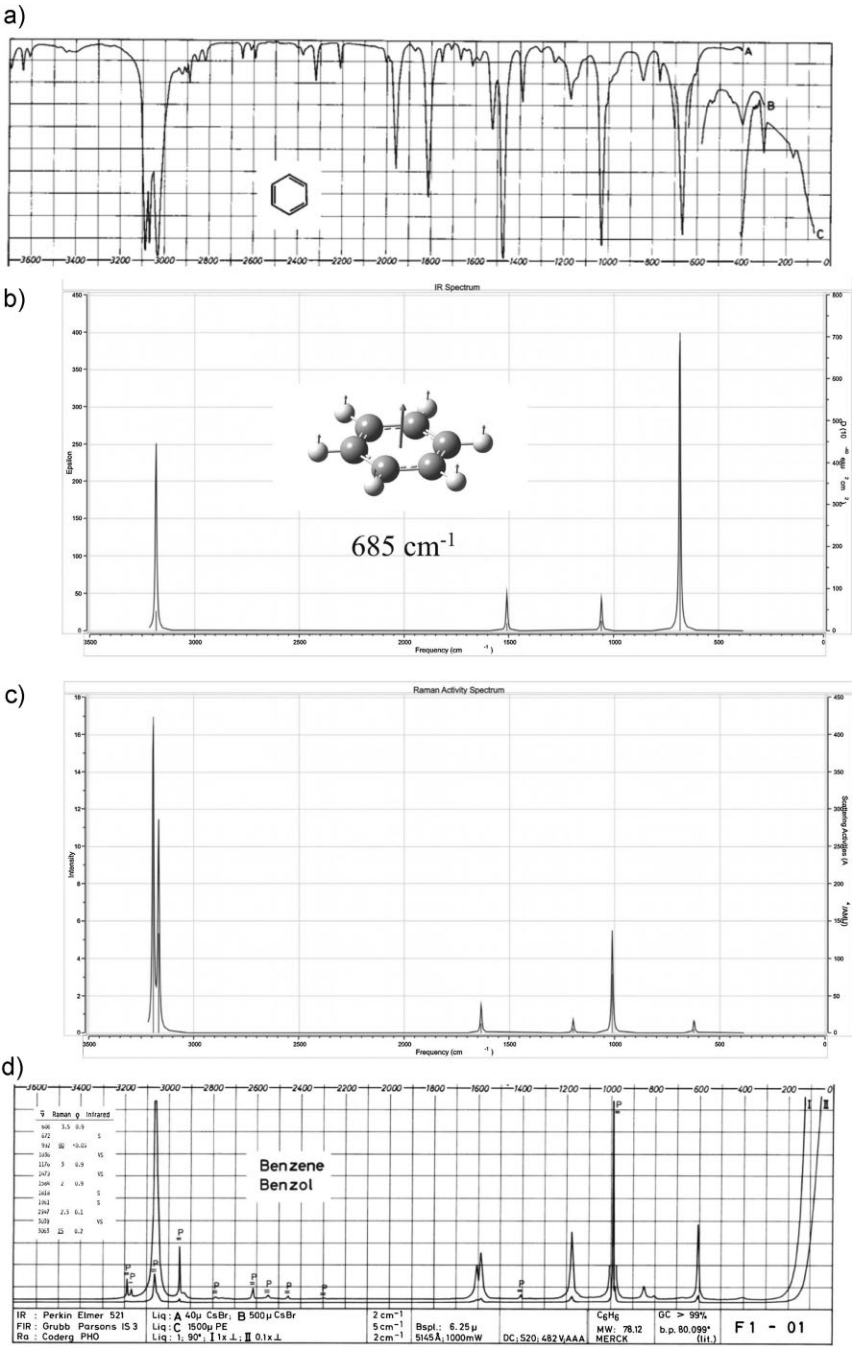

Figure 1.

Ab initio calculation of the vibrational spectra (b, c) of benzene. The calculation has been done using density functional theory (DFT: B3LYP/6-311^{++}G**) The inset shows the displacement vectors and the dipole derivative unit vector of the C-H out of plane bending vibration of benzene at 685 cm^{-1} (calculated). For comparison, the experimental IR (a) and Raman (d) spectra of benzene are shown (B. Schrader: Raman/Infrared Atlas of Organic Compounds, 2nd Edition. Page F1-01. 1989. Copyright Wiley-VCH Verlag GmbH & Co. KGaA. Reproduced with permission).

B3LYP (Becke three hybrid exchange,[12] Lee-Yang-Parr correlation[13]), employing the basis set 6-31^{++}G**. For comparison, the experimental IR and Raman spectra of benzene are shown in a) and d), resp. The calculated frequencies agree very well with the experimental spectrum, only a single factor close to 1 has to be used (e.g. $672\,cm^{-1}/685\,cm^{-1} = 0.98$) to get the experimental values from the calculated ones. To illustrate the extremely useful visualization of the vibrations, the inset shows the displacement vectors and the dipole derivative unit vector of the C-H out of plane bending vibration of benzene at $685\,cm^{-1}$ (calculated).

If the exciting radiation lies within the absorption spectrum of the sample, no normal Raman spectrum is obtained, but instead a resonance Raman spectrum will be measured. In this spectrum some bands are enhanced compared to the normal Raman, namely those of the vibrating atoms whose electrons are excited. For example, in the resonance Raman spectrum of Cytochrome c at 532 nm[14,15] only vibrational bands of the chromophor can be observed, whereas the protein part is too weak in intensity. This is also very important for the measurement of TERS. Most of the measurements published have been done on carbon allotropes[16] and dyes, all of them showing resonant Raman spectra. Measurement of the TERS of non-resonant molecules is much more difficult, and this includes normal polymers.

Method

In its normal form Raman spectroscopy uses a laser beam of ~1 mm diameter for the excitation of Raman scattering, and so its topographical resolution is limited to this value. Using a confocal microscope this limit can be reduced to about half of the wavelength of the exciting laser, e.g. 300 nm (confocal Raman spectroscopy). As for the usage in nanotechnology this value is still not good enough, it can be further reduced by tip-enhanced Raman mapping (TERM), where in a confocal Raman spectrometer a very sharp gold tip is aligned to the center of the focused laser beam. By scanning this illuminated tip over the sample, the Raman spectrum is tip-enhanced (TERS), and a topographical map with a spatial resolution of down to 15 nm with a high enhancement has been obtained.

Tip-enhanced Raman spectroscopy is the result of the large field enhancement at a noble metal tip. The field enhancement at a sharp tip arises from a combination of a quasi-static lightning-rod effect and surface-plasmon excitations. The lightning rod effect can be calculated from Maxwell's equations. These are second-order differential equations, and the fields can become singular when the first or second derivative is not defined. That would be the case for e.g. ideal conductors or infinitely sharp tips. However, real metals have finite conductivity, and the radius of curvature at the tip is finite. That means that there is no real field singularity, but the field at the tip can be strongly enhanced. The surface-plasmon excitation results from resonances in the collective electron oscillations. For a geometry as the gold tip, analytical methods cannot be used for the calculations. Instead one has to use numerical methods and computational programs using finite elements methods to get the field distributions resulting from irradiation by the laser. Several studies have been performed using different tip geometries, tip materials, and excitation conditions. As an example, Figure 2 shows the field distribution calculated by Bouhelier *et al.* [17] resulting from plane-wave excitation of a gold tip at a wavelength of $\lambda = 650\,nm$.

The calculations also show that for the enhancement of the Raman spectrum it is very important that the polarization of the light used to excite the Raman spectrum is polarized parallel to the axis of the tip (*p*-polarization, Figure 3). This produces great difficulties when irradiating the tip from below, which is normally the case.

Normally the gold tips are produced by electrochemical etching of gold wire. According to Ren *et al.* [18] a gold tip with

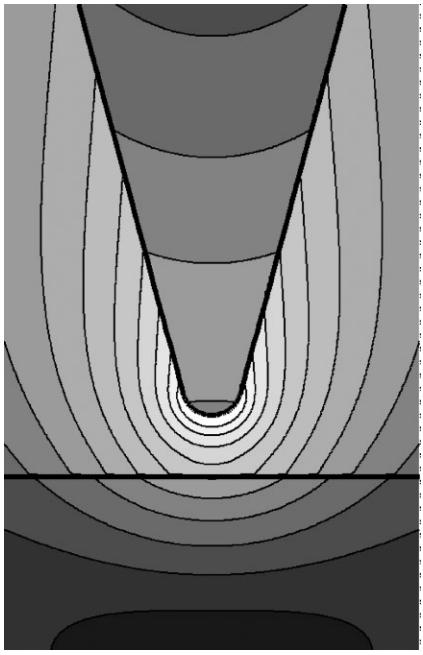

Figure 2.
Calculated field distribution [$|E(\mathbf{r}, \omega)|^2$] near a gold tip located above a glass substrate and irradiated by an on-axis focused HG_{10} laser mode. (Reprinted Figure 6 with permission from: A. Bouhelier, M. Beversluis, A. Hartschuh, L. Novotny, *Phys. Rev. Lett.* **2003**, *90*, 013903. Copyright 2003 by the American Physical Society.).

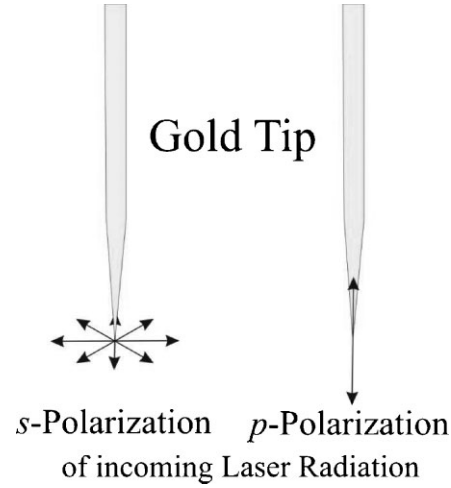

Figure 3.
Schematic Diagram of *s*- and *p*-Polarization at the tip.

a tip radius down to 10 nm is etched from a 0.2 mm gold wire using a 1:1 mixture of 37% HCl (in water) and ethanol (Figure 4). The gold wire (magnified for clarity in the scheme) is connected to the anode of the voltage source, surrounded by a 1 mm gold wire formed to a ring connected to the cathode. The etching process mainly takes place at the meniscus of the etching liquid. When the diameter of the gold wire's

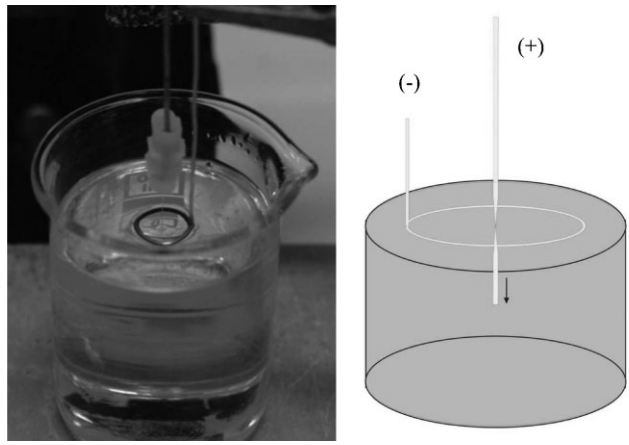

Figure 4.
Photo (left) and scheme (right) of the etching of the gold tip. A 0.2 mm gold wire (magnified for clarity in the scheme) is connected to the anode of the voltage source, surrounded by a 1 mm gold wire formed to a ring connected to the cathode. The etching process mainly takes place at the meniscus of the etching liquid. When the diameter of the gold wire's waistline is thin enough, the lower part will drop by its own weight.

waistline is small enough, the lower part will drop by its own weight. This can be nicely seen from the electron microscopic image in Figure 5. The rough body of the wire (produced by a slightly mismatched voltage) is etched electrochemically, while the smooth tip is drawn by the weight of the lower part of the wire.

In contrast to the method of producing tips by electrochemically etching silver or gold wires, TERS tips can also be produced by sputtering AFM tips with silver or gold *in vacuo*. Figure 6 shows such a silver coated AFM tip at increasing magnifications. At the highest magnification, the Ag clusters at the tip are clearly visible, and one can easily imagine that the actual enhancement of such a tip is strongly dependant on the exact placement of the clusters. Experimentally it is found that coated AFM tips give much less enhancement than etched tips (see Figure 11).

In the principal TERS experiment (Figure 7) a transparent sample on a thin glass support is measured with a laser beam (from below) focused by a high numerical aperture (NA) objective on the sample. The higher the NA of the objective, the stronger are the *p*-polarized components of the exciting light beam, thereby circumventing the aforementioned difficulties. In the center of the focus a sharp gold tip, attached to a vibrating tuning fork, is placed. The distance of the tip is kept constant by a feedback loop to a piezo drive for the Z-direction, and the displacement for the mapping is done by a high precision XY-stage. The enhanced Raman spectrum is collected by the objective and fed into the spectrometer.

For opaque samples the basic TERS experiment has to be modified using side illumination (Figure 8). Again a laser beam is focused by a high numerical aperture objective on the sample, this time using an angle of 60° to the tip axis.

The layout of our scanning near-field optical Spectrometer (''Nanofinder'', NT-MDT, Moskow, Russia, Photo Figure 9) is shown in Figure 10. An inverted microscope is coupled to a spectrometer of the Cherny-Turner type, the light collected by the objective focused on its way through a pinhole, thereby allowing for confocal Raman measurements. The Raman radiation is freed from Rayleigh scattering by an edge and a notch filter, then detected by a Peltier-cooled, backthinned CCD-detector. A photomultiplier (PMT) receives about 3% of the light from a beamsplitter, which allows for the imaging of the reflection from the tip. The XY-stage has to have a very

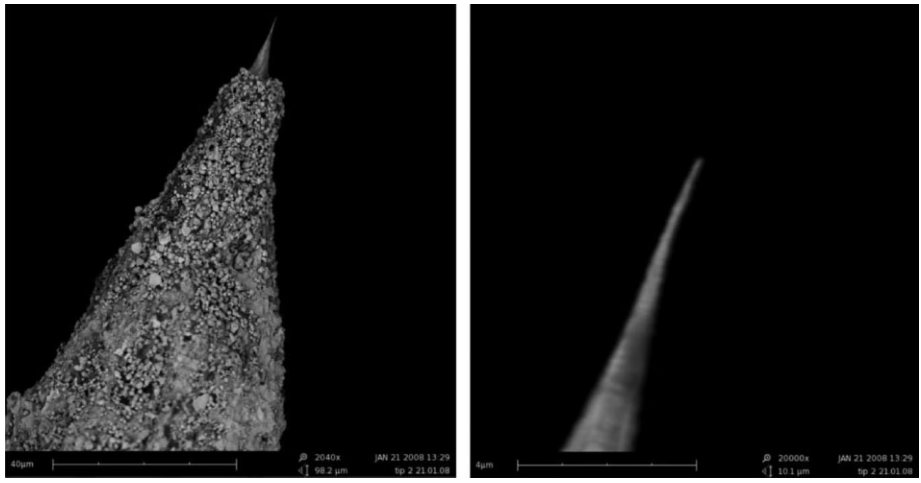

Figure 5.
Electrochemically etched gold tip at low (left) and high (right) magnification. The figure clearly shows that the last fine part is drawn by the weight of the lower part of the wire.

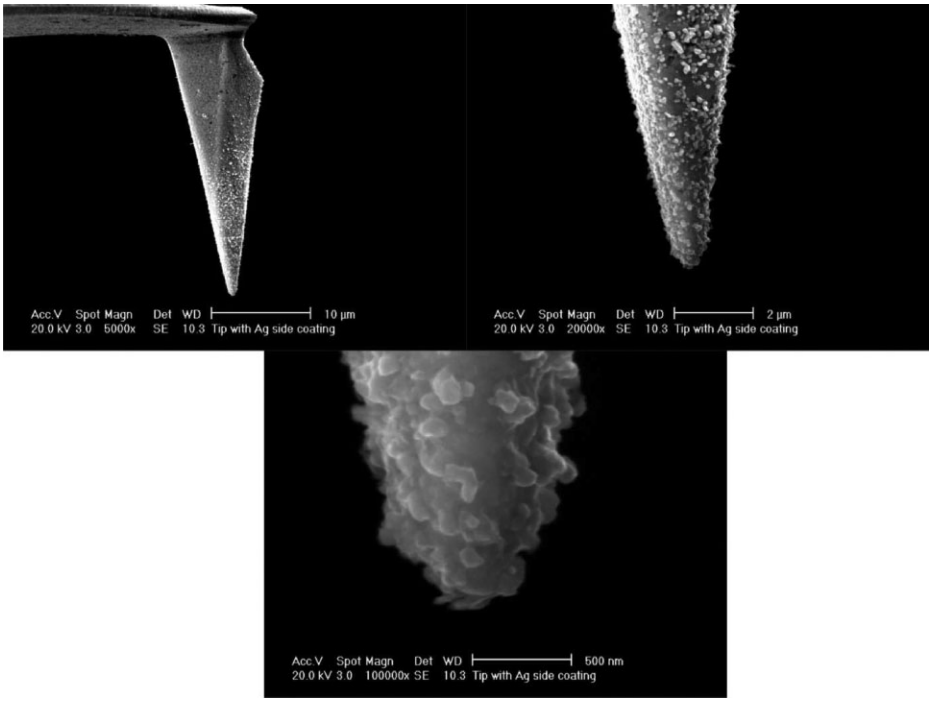

Figure 6.
Silver-coated AFM tip at increasing magnifications. At the highest magnification, the Ag clusters at the tip are clearly visible.

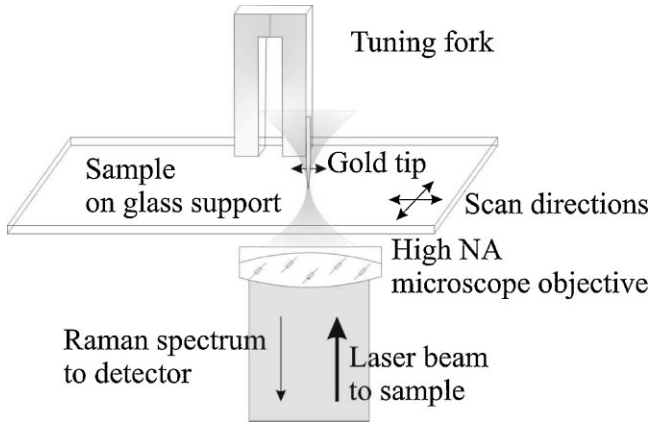

Figure 7.
Principal TERS experiment, showing the measurement of a transparent sample on a thin glass support. A laser beam (from below) is focused by a high numerical aperture objective on the sample. In the center of the focus a sharp gold tip, attached to a vibrating tuning fork, is placed. The distance of the tip is kept constant by a feedback loop to a piezo, and the mapping is done by a high precision XY-stage. The enhanced Raman spectrum is collected by the objective and fed into the spectrometer.

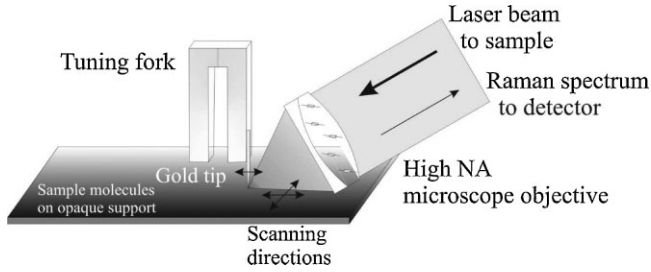

Figure 8.
TERM configuration for opaque samples (side illumination). A laser beam is focused by a high numerical aperture objective on the sample, this time using an angle of 60° to the tip axis. The other arrangements are the same as in the basic TERM experiment.

high stability, as when taking high-resolution TERM images for hours to days, it may only deviate from the desired position by a few nanometers.

Tip-Enhanced Raman Mapping (TERM)

As the mapping using TERS needs good enhancement and a very stable XY-table, it is a very challenging experiment and since it takes from tens of hours to several days, very few examples are known from the literature. We will present them in the following together with some new results from our laboratory.

TERS of Single-Wall Carbon Nanotubes

Nowadays, single-wall carbon nanotubes (SWNTs) play a significant role in nanotechnology research and the development of electrically conductive composite polymers. SWNTs show mainly three characteristic Raman bands: the radial breathing mode (RBM, 100–300 cm^{-1}), the tangential stretching mode (G band, ~1600 cm^{-1}) and the disorder induced mode (D band, ~1300 cm^{-1}). Figure 11 shows the near and far field spectra of a bundle of single-wall carbon nanotubes. The far field spectrum of this bundle in A (dashed line) is enhanced using a gold-sputtered cantilever by a factor of 12 (432 area corrected, solid line) for the D band and in B enhanced

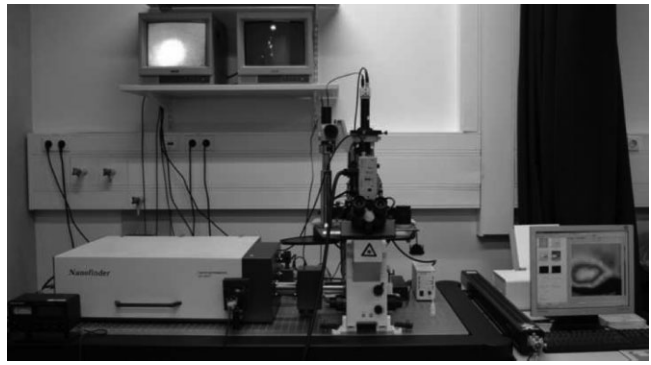

Figure 9.
TERM setup at the Eindhoven University of Technology, showing the inverted microscope with the shear force head (middle), the Raman spectrometer (Nanofinder, left), and the HeNe laser (right, next to the computer screen). The experiment can be observed from below and from the side by cameras on the microscope and the monitors seen on top.

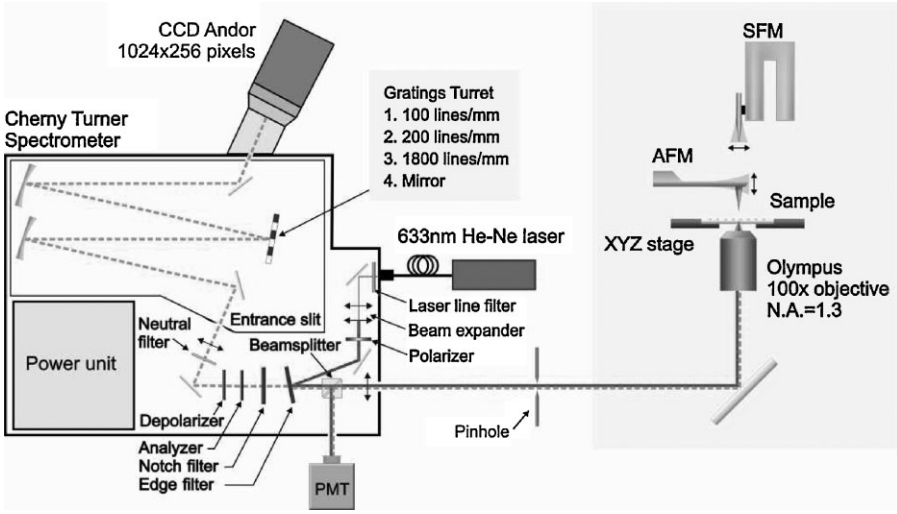

Figure 10.
Layout of our scanning Near-Field optical Spectrometer (''Nanofinder'' from NT-MDT), inverted configuration, reproduced by permission from: S. S. Kharintsev, G. G. Hoffmann, P. S. Dorozhkin, G. de With, J. Loos, *Nanotechnology*, **2007**, *18*, 315502. ©2007 IOP).

by an etched gold wire by a factor of 263 (105000 area corrected) for the *G* band. Consequently for the TERM on carbon nanotubes we took an etched gold wire glued to a quartz tuning fork.[19,20]

Figure 12 shows the TERM of a bundle of single-wall carbon nanotubes, using the RBM-line (A), the *D*-line (B), and the *G*-line (C). For comparison, the confocal Raman mapping using the different lines is shown in column I. Column III shows a cross-section indicated by the white line in II. From these cross-sections the resolution of the TERM can be estimated to be below 50 nm (35 nm from a Gaussian fit), as opposed to about 300 nm in the confocal scans.

Using the high resolution of TERS, even defects in a single SWCNT can be detected. Hartschuh *et al.*[21] performed TERS experiments along a single SWCNT (grown by arc discharge using a Ni/Y catalyst)

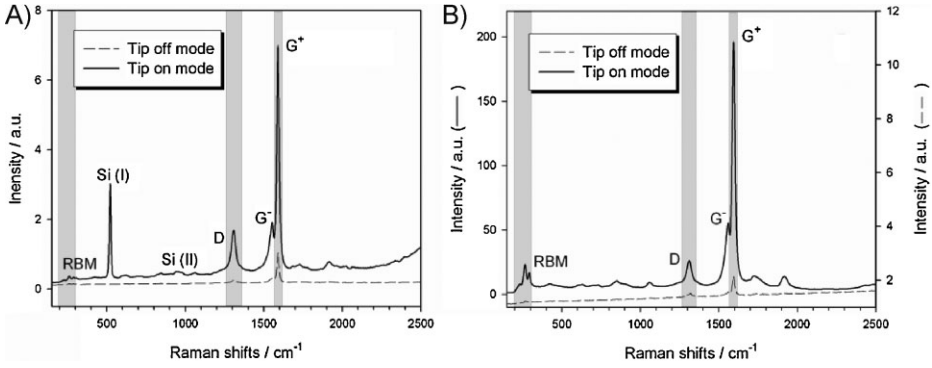

Figure 11.
TERS of a bundle of single-walled carbon nanotubes, showing the enhancement by a gold coated cantilever (A) and by an etched gold wire (B). Note the different intensity scales for the the far field (without tip) and near field (tip landed) spectra in B. (reproduced by permission from: S. S. Kharintsev, G. G. Hoffmann, P. S. Dorozhkin, G. de With, J. Loos, *Nanotechnology*, **2007**, *18*, 315502. ©2007 IOP).

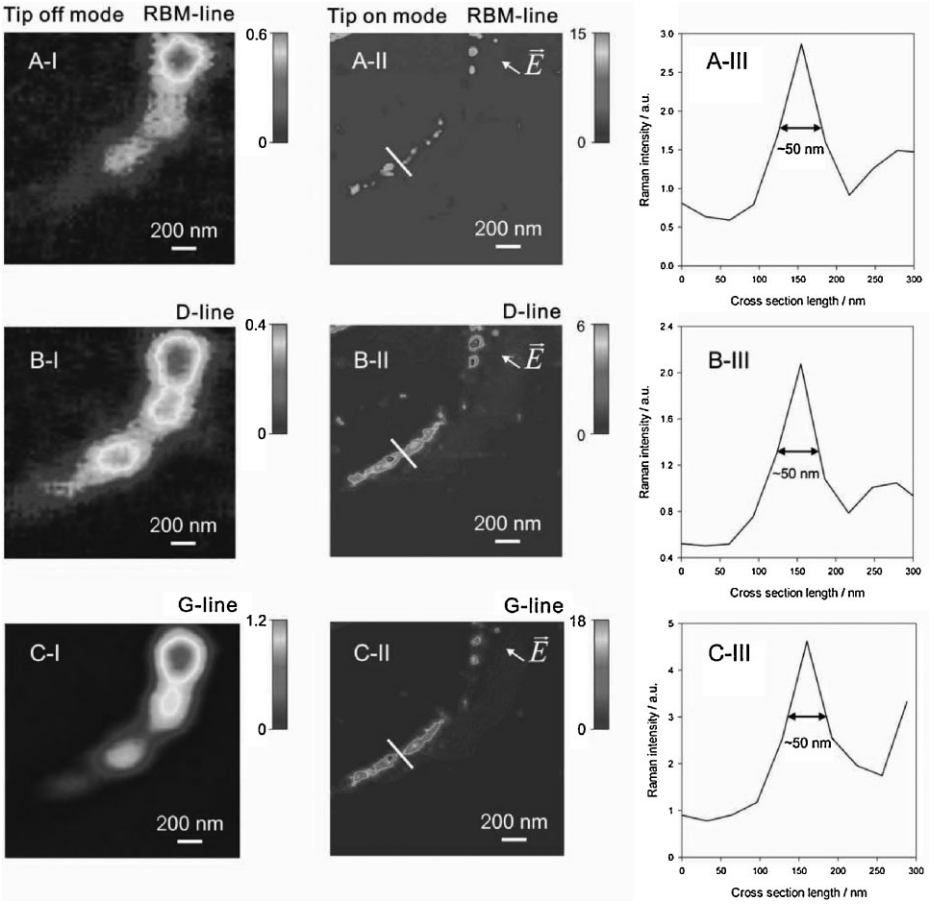

Figure 12.
TERM of a bundle of single-walled Carbon Nanotubes, using the RBM-line (A), the *D*-line (B), and the *G*-line (C), (III) showing a cross section indicated by the white line in II (reproduced by permission from: S. S. Kharintsev, G. G. Hoffmann, P. S. Dorozhkin, G. de With, J. Loos, *Nanotechnology* **2007**, *18*, 315502. © 2007 IOP).

at 4 adjacent positions (Figure 13). At the beginning of the SWCNT, positions 1 and 2, the *G* band shows a stronger intensity than the *2D* band at $\sim 2600\,\mathrm{cm}^{-1}$ ($G/2D \approx 1.3$). By measuring along the SWCNT (positions 3 and 4), the intensity of the G band decreases compared to the *2D* band ($G/2D \approx 0.7$). A frequency shift in the band position has not been observed for the *G* band, but shifts of significant strength were detected for the *2D* band. The spectral fluctuations represent changes in the SWCNT structure, which can be related to external stress produced by local defects or particles from the catalyst. Such results cannot be provided by any other method and again indicate the potential of TERS measurements.

TERS of a Monolayer (Depth Profiling)

As it is well known that the curve of the enhancement factor versus tip-sample distance (Figure 14, Kharintsev *et al.*[19] and references cited therein) is very steep at close distances, it seemed interesting to try TERS on monolayers of the Langmuir-Blodgett type, to do some type of depth profiling. Indeed, our first experiments showed a large distance-related change in the TER spectra of a N-alkyl dopamine derivative, which was transferred onto a glass substrate.[22] Due to the complicated

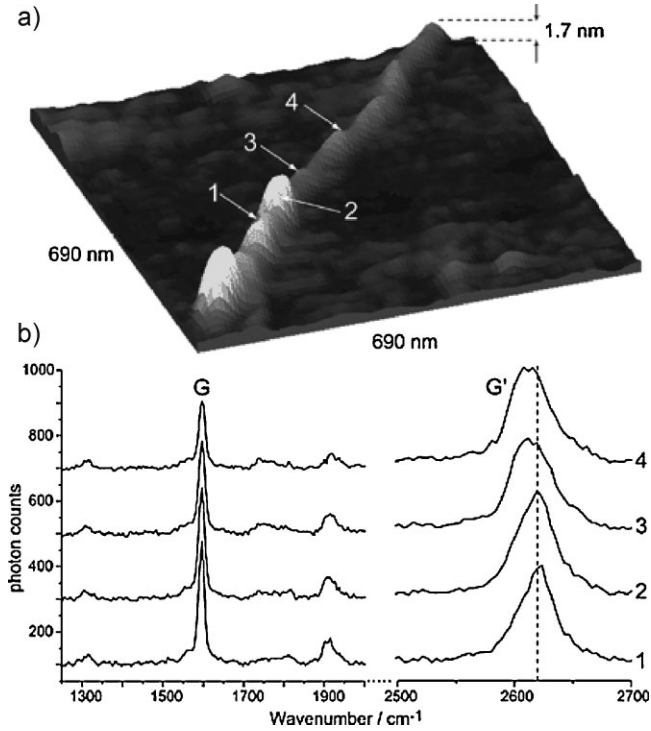

Figure 13.
TERS experiments along a single SWCNT at 4 adjacent positions. At the beginning of the SWCNT, positions 1 and 2, the *G* band shows a stronger intensity than the *2D* band (reproduced from A. Hartschuh, E. J. Sánchez, X. S. Xie and L. Novotny, *Phys. Rev. Lett.* **2003**, *90*, 095503, by kind permission of the author and IOP).

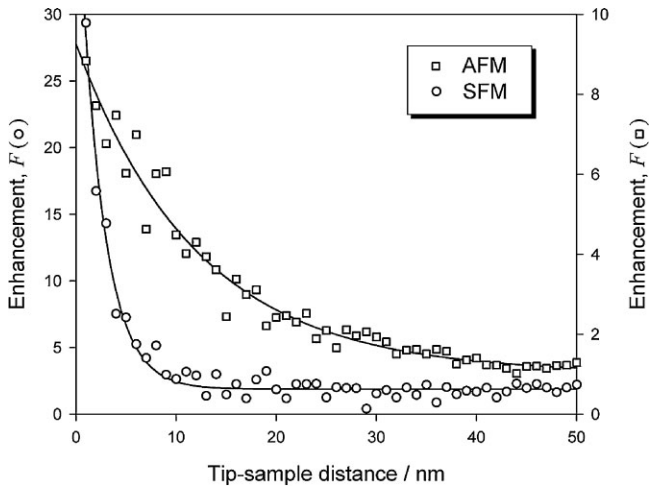

Figure 14.
Enhancement factor *versus* tip-sample distance (reproduced by permission from: S. S. Kharintsev, G. G. Hoffmann, P. S. Dorozhkin, G. de With, J. Loos, *Nanotechnology* **2007**, *18*, 315502. ©2007 IOP).

nature of the Raman spectra of larger molecules, interpretation of the results is not straightforward and has to be accompanied by high quality *ab initio* calculations.

TERS Mapping of Graphene

As carbon nanotubes, another of the allotropes of carbon, graphene, is of great interest for composite polymers. It strengthens polymers, and in the case of conductive polymers, performs even better than carbon nanotubes. The ''graphene'' used as filler for polymers is produced by oxidative exfoliation of graphite, followed by the reduction of the resulting graphene oxide. For the analysis of the completion of the oxidation/reduction cycle Raman analysis is used advantageously. Graphene also holds great promise as a material for electronic devices due to the high electron mobility in this structure. Recently, Liao *et al.*[23] reported the production of a high-speed transistor using graphene. Microwave measurements on these transistors show an intrinsic cut-off frequency in the range of 100–300 GHz, which is about twice as fast as the very best silicon MOSFETs of a similar size (Figure 15).

Figure 16a) and b) show the 633 nm Raman spectra of graphene and graphite (>3 layers) resp. The two most intense features for graphite are the *G* peak at $\sim 1575\,cm^{-1}$ and the *2D* peak at $\sim 2681\,cm^{-1}$. The *G* band is a tangential shear mode of carbon atoms that corresponds to the stretching mode in the graphite plane. The *G* peak is due to the doubly degenerate zone center *E2g* mode. The *2D* band is a second-order process from two zone boundary LO phonons. It is an intrinsic property of graphite, and present even in defect-free structures. Since zone-boundary phonons do not satisfy the Raman fundamental selection rule, they are not seen in first order Raman spectra of defect-free graphite, but they give rise to a peak at $\sim 1350\,cm^{-1}$ in defect containing graphite, called the *D* peak.

The spectra in Figure 16 show a significant change in shape and intensity of the 2*D* peak of graphene as compared to bulk graphite. The *2D* peak in bulk graphite presents a shoulder and a main peak of roughly one fourth of the height of the *G* peak. We measure a single, sharp 2*D* peak in graphene, roughly 5 times more intense than the *G* peak. In detail, it is possible to see the evolution of the 2*D* band as a function of number of layers analyzed. This immediately indicates that a bilayer has a much broader and up-shifted *2D* band with respect to graphene. For more than five layers the Raman spectrum becomes hardly distinguishable from that of bulk graphite.[24] It should be mentioned that so far it has not been proven absolutely by complementary techniques that shape and position of the *2D* band originates really from a single graphene sheet.

A high resolution TERM of mechanically cleaved graphene is given in Figure 17a), showing the area of the zoom-in b) as a black frame.[25] In a) and

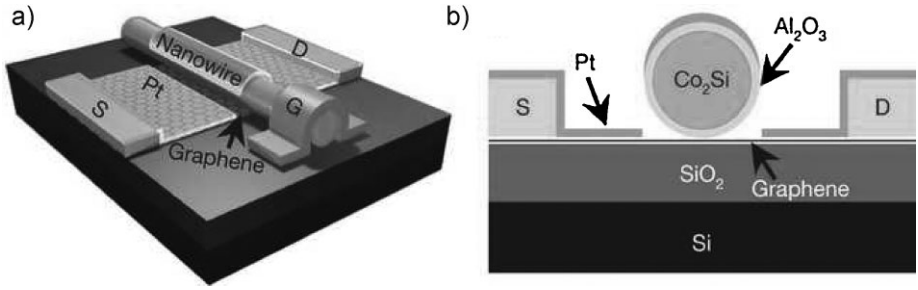

Figure 15.
Graphene transistor using a self-adjusting Co_2Si nanowire as the gate (G), platinum as the contact from graphene to the drain (D) and source (S). Reprinted by permission from Macmillan Publishers Ltd: L. Liao, Y.-C. Lin, M. Bao, R. Cheng, J. Bai, Y. Liu, Y. Qu, K. L. Wang, Y. Huang, X. Duan, *Nature* ***467***, 305–308. Copyright 2010.

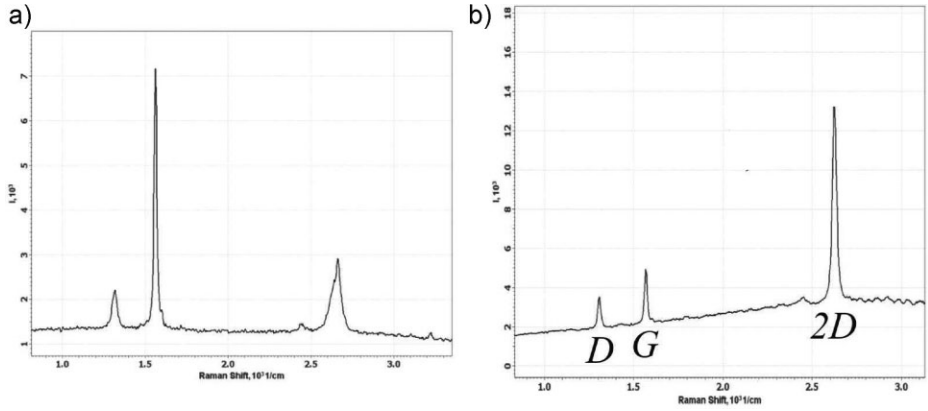

Figure 16.
Raman spectra of a) graphite and b) graphene, showing the position of the *D*, *G*, and *2D* bands.

b) the center position of the *2D* Raman line is color coded. For comparison, an optical microscopic reflection image is given in c). As expected, no graphene can be detected in the optical reflection image c), but the TERM on graphene clearly shows the single layer graphene sheet as a black area in Figure 17a) and b), surrounded by 2-layer and 3-layer graphite. The spatial resolution of the TERM is better than 60 nm.

TERS Mapping of DNA

One of the dreams of the TERS researchers is the direct reading of the base pair sequence of nucleic acids. As a first step toward this goal Bailo and Deckert[26] measured the TERS of a single strand of RNA with only one type of nucleoside at different places. As a second step we recently realized the first TERM on a sample of plasmid DNA[27] firmly attached to a mica substrate using Ni^{2+}-ions. An AFM phase image of the ring-shaped molecules is shown in Figure 18. It was measured using an AFM cantilever equipped with a diamond-like carbon (DLC) whisker, featuring a tip radius of 1 nm. The TERS measurement using the vibrational line of the phosphate

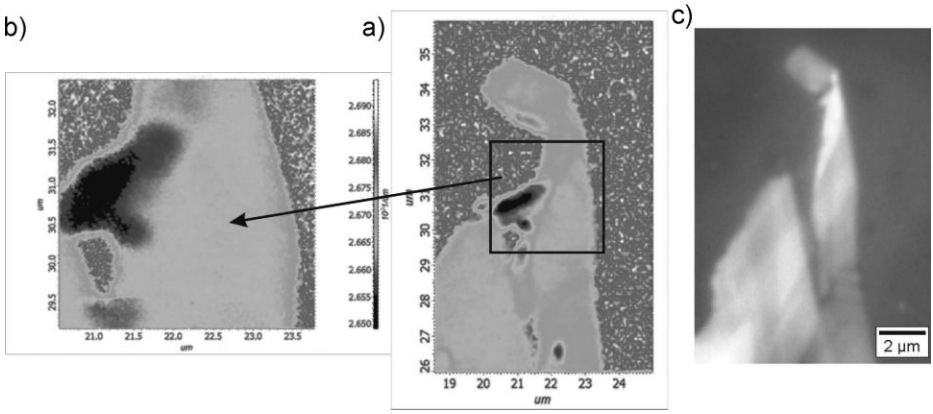

Figure 17.
TERM of mechanically cleaved graphene. A low resolution TERM is given in a), showing the area of the zoom in b) as a black frame. In b) the center position of the *2D* Raman line is colour coded, where black means graphene. For comparison, an optical microscopic reflection image is given in c).

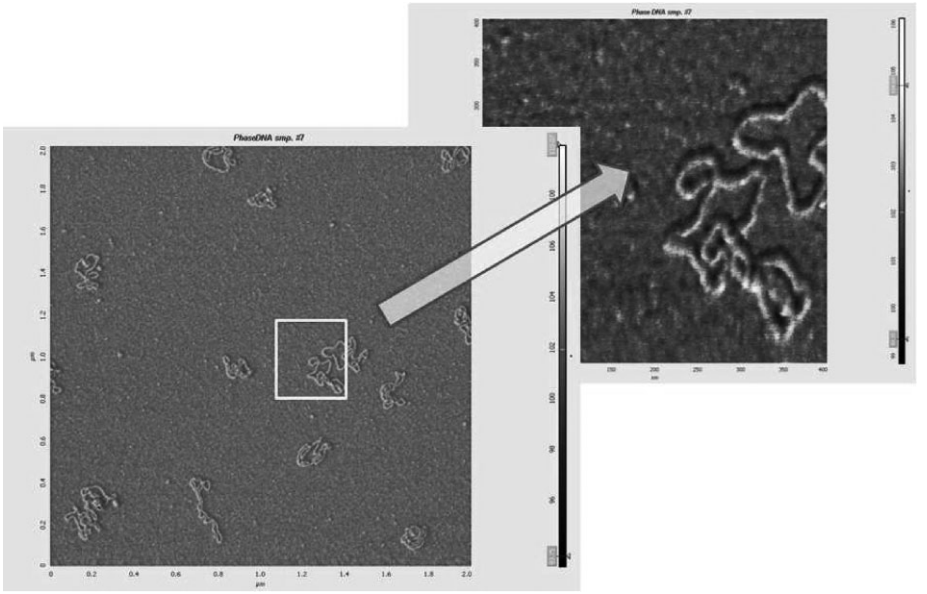

Figure 18.
AFM image of a circular plasmid DNA molecule.

residues at $1092\,cm^{-1}$ (PO_2^-) shows an ovaloid shape of the correct size: long axis 300 nm, short axis 150 nm. Work on higher resolution is in progress.

TERS Mapping of Polymers

To obtain the desired mechanical and functional properties of thin polymer films (used for e.g. packaging materials, sensors, and membranes) different polymers are blended together. Of course, it is not desirable that during the lifetime of the blend phase separation occurs. Therefore, detailed knowledge of phase separation behaviour is extracted from experiments at elevated temperatures. Figure 19 shows a microscopic image of such a PMMA/SAN polymer blend thin film, as it can be seen by the camera of the inverted microscope of our Nanofinder. It shows a PMMA/SAN block copolymer annealed at 250 °C for 5 min. Also a gold tip can be seen, landed on it. Only the tiny dark-black spot corresponds to the image of the tip apex, the somewhat lighter cone is the shadow of the rest of the tip. For the same film the TERM image is shown in Figure 20. The TERM has been produced using the maximum Raman intensity of the Raman bands (a) at $1002\,cm^{-1}$ corresponding to SAN and (b) at $800\,cm^{-1}$ corresponding to PMMA. This film shows a late stage of phase separation.

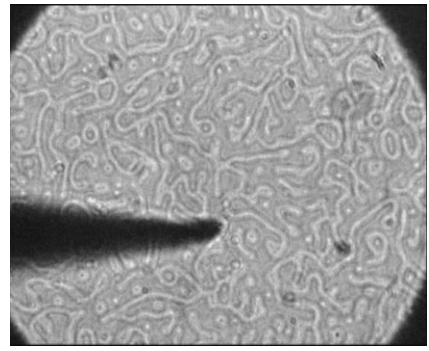

Figure 19.
A gold tip, landed on a PMMA/SAN polymer blend film, can be seen by the camera of the inverted microscope of our Nanofinder. Only the tiny dark-black spot corresponds to the image of the tip apex, the somewhat lighter cone is the shadow of the rest of the tip.

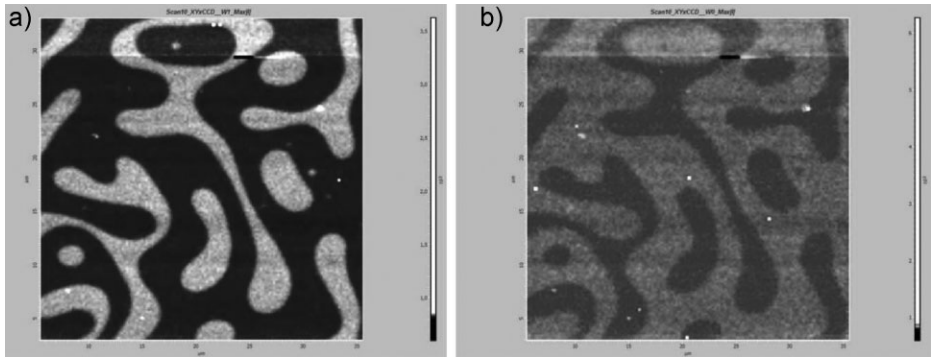

Figure 20.
TERM of a thin film of a PMMA/SAN block copolymer annealed at 250 °C for 5 min, showing the maximum Raman intensity of the Raman bands (a) at 1002 cm^{-1} corresponding to SAN and (b) at 800 cm^{-1} corresponding to PMMA.

Figure 21 shows a TERM of a thin film at an early stage of phase separation. Here the PMMA/SAN block copolymer was annealed at 250 °C for only 2 min, showing the maximum Raman intensity of the Raman band at 1002 cm^{-1} corresponding to SAN. Most interesting is the thin interface between both phases. It was measured to be about 200 nm in width[28].

Outlook

The most important part, and also the greatest problem in tip-enhanced Raman

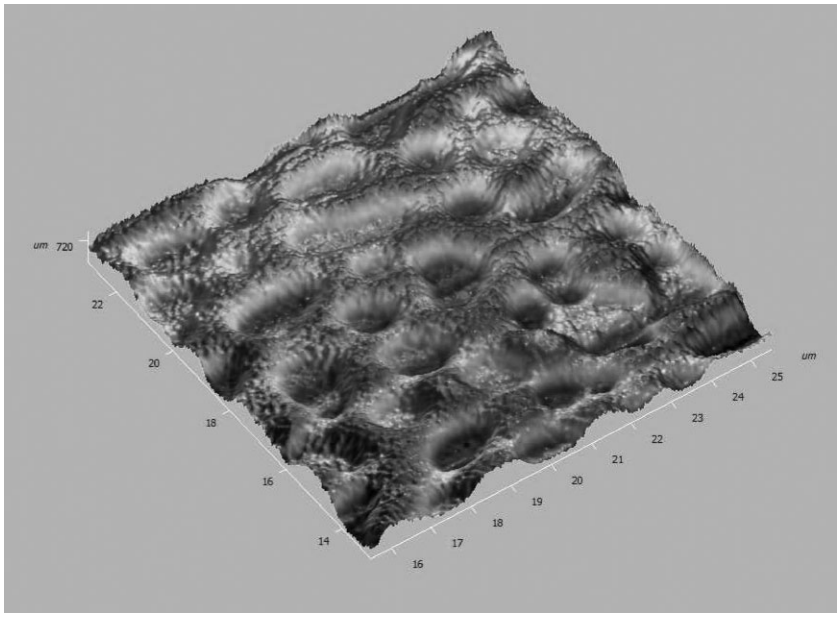

Figure 21.
TERM of a thin film of a PMMA/SAN block copolymer annealed at 250 °C for 2 min, showing the maximum Raman intensity of the Raman band at 1002 cm^{-1} corresponding to SAN.

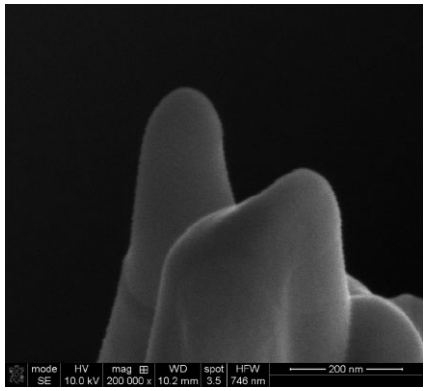

Figure 22.
End of a gold wire sharpened to a fine, smooth tip by a fast beam of Gallium ions.

spectroscopy, is the tip. In particular, the gold tips are very soft and can easily be damaged, whereas the silver tips are prone to poisoning by sulfur compounds. So a number of techniques have been applied to prepare (hopefully) improved TERS tips.

In the scanning electron microscope (SEM) milling can be achieved using fast ion bombardment (FIB).[29] Normally a stream of highly accelerated Gallium ions is used for this purpose.

A very promising technique is the sharpening of a gold wire or, to save time, a pre-etched gold tip. In Figure 22 we see the nicely shaped, smooth tip milled by a fast beam of Gallium ions. Figure 23a) and b) shows a used gold tip showing bent and polluted and (c and d) then refurbished and sharpened.

As an alternative approach, material is not taken away, but instead build up on a substrate. In Figure 24 an AFM tip is pictured in high magnification, showing Pt piles, electron-beam deposited from a

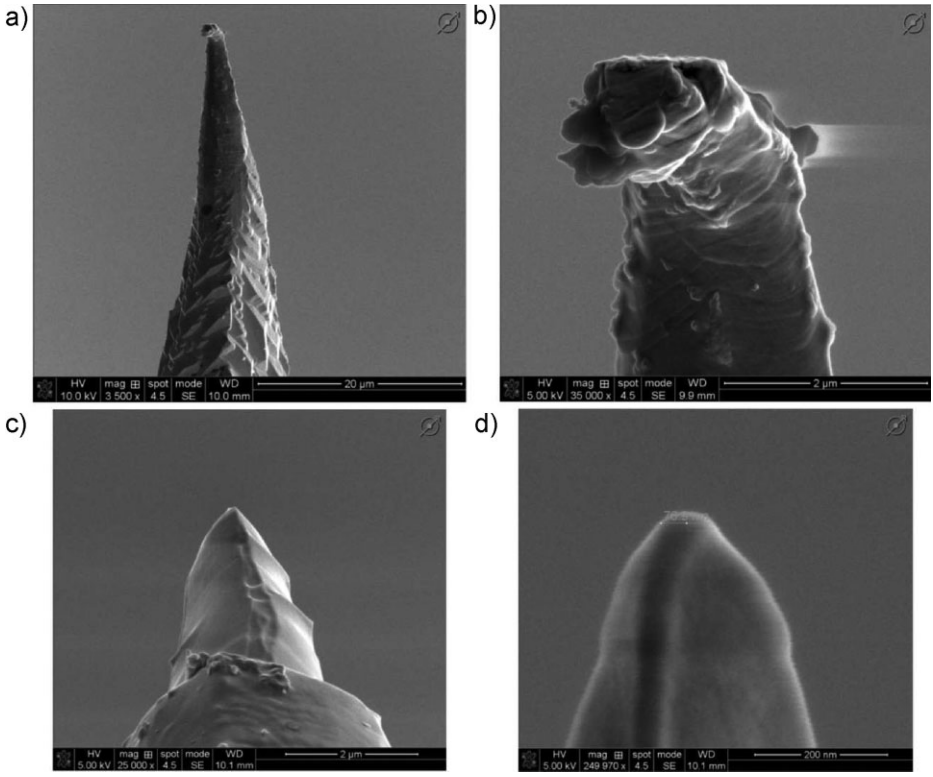

Figure 23.
A used gold tip [a) low, b) high magnification] is bent and polluted. FIB milling [c) low, d) high magnification] sharpens it again.

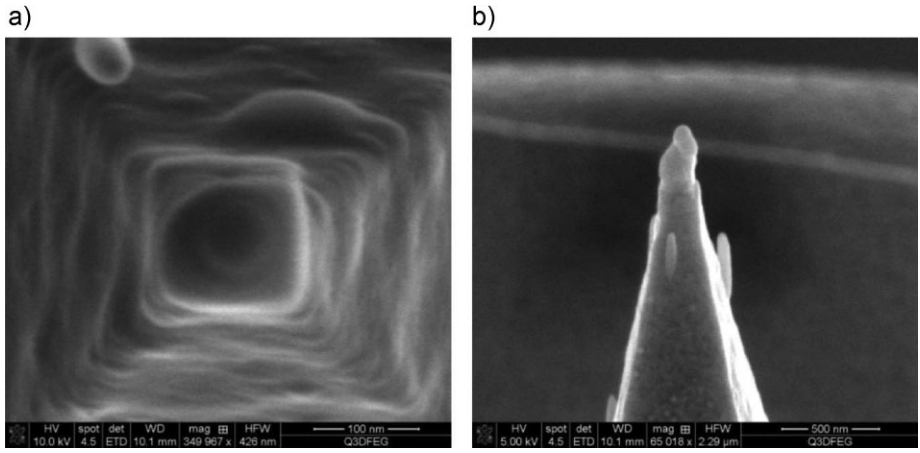

Figure 24.
AFM tip with electron-beam deposited Pt piles. a) top view b) side view.

gaseous precursor. Such a precursor is also available for gold.

Acknowledgements: We gratefully acknowledge financial support by the Dutch Polymer Institute (DPI, grant #692). We also thank Marcos Ghomez Ghislandi fort the graphene sample, Dina Ribena for the monolayer sample, Sergey S. Kharintsev for the TERS experiments on SWCNTs, and Niek J. H. G. M. Lousberg for the SEM images and FIB and EBID work.

[1] S. Kawata, ''*Near-field Optics and Surface Plasmon Polaritons*'', Springer, Berlin **2001**.
[2] S. Kawata, M. Ohtsu, M. Irie, ''*Nano-Optics*'', Springer, Berlin **2002**.
[3] D. Courjon, ''*Near-Field Microscopy and Near-Field Optics*'', Imperial College Press, London **2003**.
[4] A. Hartschuh, M. Beversluis, A. Bouhelier, L. Novotny, *Phil. Trans. R. Soc.* **2004**, *362*, 807.
[5] P. N. Prasad, ''*Nanophotonics*'', Wiley, New York **2004**.
[6] L. Novotny, S. J. Stranick, *Annual Review of Physical Chem.* **2006**, *57*, 303.
[7] B. Schrader, ''*Raman/Infrared Atlas of Organic Compounds*'', 2nd Edition, VCH, Weinheim **1989**.
[8] B. Schrader, Ed., ''*Infrared and Raman Spectroscopy*'', VCH, Weinheim **1995**.
[9] G. G. Hoffmann, in: ''*Encyclopedia of Spectroscopy and Spectrometry*'', 2nd Edition, J. Lindon, G. Tranter and J. Holmes, Eds., Academic Press, London **2010**, 1738.
[10] G.G. Hoffmann, in: ''*Encyclopedia of Spectroscopy and Spectrometry*'', 2nd Edition, J. Lindon, G. Tranter and J. Holmes, Eds., Academic Press, London **2010**, 2349.
[11] *Gaussian09*, Revision A.02; M. J. Frisch, G. W. Trucks, H. B. Schlegel, G. E. Scuseria, M. A. Robb, J. R. Cheeseman, G. Scalmani, V. Barone, B. Mennucci, G. A. Petersson, H. Nakatsuji, M. Caricato, X. Li, H. P. Hratchian, A. F. Izmaylov, J. Bloino, G. Zheng, J. L. Sonnenberg, M. Hada, M. Ehara, K. Toyota, R. Fukuda, J. Hasegawa, M. Ishida, T. Nakajima, Y. Honda, O. Kitao, H. Nakai, T. Vreven, J. A. Montgomery, Jr., J. E. Peralta, F. Ogliaro, M. Bearpark, J. J. Heyd, E. Brothers, K. N. Kudin, V. N. Staroverov, R. Kobayashi, J. Normand, K. Raghavachari, A. Rendell, J. C. Burant, S. S. Iyengar, J. Tomasi, M. Cossi, N. Rega, J. M. Millam, M. Klene, J. E. Knox, J. B. Cross, V. Bakken, C. Adamo, J. Jaramillo, R. Gomperts, R. E. Stratmann, O. Yazyev, A. J. Austin, R. Cammi, C. Pomelli, J. W. Ochterski, R. L. Martin, K. Morokuma, V. G. Zakrzewski, G. A. Voth, P. Salvador, J. J. Dannenberg, S. Dapprich, A. D. Daniels, O. Farkas, J. B. Foresman, J. V. Ortiz, J. Cioslowski, D. J. Fox, *Gaussian, Inc., Wallingford CT* **2009**.
[12] A. D. Becke, *J. Chem. Phys.* **1993**, *98*, 5648.
[13] C. Lee, W. Yang, R. G. Parr, *Phys. Rev. B* **1988**, *37*, 785.
[14] C. Johannessen, P. C. White, S. Abdali, *J. Phys. Chem. A* **2007**, *111*(32), 7771.
[15] B.-S. Yeo, S. Mädler, T. Schmid, W. Zhang, R. Zenobi, *J. Phys. Chem. C* **2008**, *112*, 4867.
[16] G. G. Hoffmann, G. de With, J. Loos, *Macromol. Symp.* **2008**, *265*(1), 1.
[17] A. Bouhelier, M. Beversluis, A. Hartschuh, L. Novotny, *Phys. Rev. Lett.* **2003**, *90*, 013903.
[18] B. Ren, G. Picardi, B. Pettinger, *Rev. Sci. Instrum.* **2004**, *75*, 837.

[19] S. S. Kharintsev, G. G. Hoffmann, P. S. Dorozhkin, G. de With, J. Loos, *Nanotechnology* **2007**, *18*, 315502.
[20] S. S. Kharintsev, G. G. Hoffmann, J. Loos, G. de With, P. S. Dorozhkin, M. Kh. Salakhov, *J. Exp. Theor. Phys.* **2007**, *105*, 1.
[21] A. Hartschuh, E. J. Sánchez, X. S. Xie, L. Novotny, *Phys. Rev. Lett.* **2003**, *90*, 095503.
[22] G. G. Hoffmann, D. Ribena, L. Xue, J. Loos, N. A. J. M. Sommerdijk, G. de With, unpublished results.
[23] L. Liao, Y.-C. Lin, M. Bao, R. Cheng, J. Bai, Y. Liu, Y. Qu, K. L. Wang, Y. Huang, X. Duan, *Nature.* **2010**, *467*, 305.
[24] Y. Wang, Z. Ni, Z. X. Shen, H. Wang, Y. Wu, W. Chen, A. T. S. Wee, *J. Phys. Chem. C* **2008**, *112*, 10637.
[25] G. G. Hoffmann, M. G. Ghislandi, L. Xue, J. Loos, G. de With, unpublished results.
[26] E. Bailo, V. Deckert, *Angew. Chem., Int. Ed.*, **2008**, *47*, 1658.
[27] G. G. Hoffmann, L. Xue, J. Loos, G. de With, unpublished results.
[28] L. Xue, W. Li, G. G. Hoffmann, J. G. P. Goossens, J. Loos, G. de With, *Macromolecules* **2011**, *44*, in print.
[29] E. J. Sànchez, J. T. Krug II, X. S. Xie, *Rev. Sci. Instrum.* **2002**, *73*, 3901.

